Coda Q in Different Tectonic Areas, Influence of Processing Parameters

Article *in* Bulletin of the Seismological Society of America · May 2016

DOI: 10.1785/0120150359

6 authors, including:

Mathilde B. Sørensen
University of Bergen
62 PUBLICATIONS **1,664** CITATIONS
SEE PROFILE

Dina Vales
Instituto Português do Mar e da Atmosfera
31 PUBLICATIONS **251** CITATIONS
SEE PROFILE

Mehmet Özyazıcıoğlu
Ataturk University
15 PUBLICATIONS **140** CITATIONS
SEE PROFILE

Gerardo Sánchez
National University of San Juan
10 PUBLICATIONS **159** CITATIONS
SEE PROFILE

Bulletin of the Seismological Society of America, Vol. 106, No. 3, pp. –, June 2016, doi: 10.1785/0120150359

Coda Q in Different Tectonic Areas, Influence of Processing Parameters

by Jens Havskov, Mathilde B. Sørensen, Dina Vales, Mehmet Özyazıcıoğlu, Gerardo Sánchez, and Bin Li*

Abstract Published results of coda Q show a large variation in values. These variations are often claimed to be related to different tectonics, whereas they might just be related to using different assumptions in the processing, leading to different input parameters for the analysis. In this study, the effect of using different processing parameters is investigated and significant differences, particularly at low frequencies, are observed. We find a new set of optimal parameters, which we recommend using in future studies. Using a short lapse time of 30 s and optimal parameters, data from both similar and very different tectonic regions are used to calculate coda Q using the same program and the same parameters. The regions considered are eastern Anatolia, the Azores, Jan Mayen, northwestern and central Argentina, the Shanxi rift system in China, and southwestern Norway. We obtain the following relations: eastern Anatolia ($Q = 88\,f^{0.66}$), Azores ($Q = 86\,f^{0.70}$), Jan Mayen ($Q = 90\,f^{0.72}$), northwestern and central Argentina ($Q = 89\,f^{0.94}$), Shanxi rift system ($Q = 99\,f^{0.89}$), and southwestern Norway ($Q = 124\,f^{0.91}$).

The results show that coda Q is very similar for regions of similar tectonics and significantly different for regions with varying tectonics. Using alternative, more common parameters gives different Q, but the regional differences remain, so which parameters to use to get correct coda Q values is still uncertain. However, coda Q can clearly distinguish different tectonic areas provided identical processing parameters are used, even if they are not optimal.

Introduction

Seismic attenuation estimates calculated from the decay of coda waves have been described and evaluated many times since the introduction by Aki and Chouet (1975) of this approach. This coda Q method can give quite different results depending on the processing parameters used. Many papers have been published that claim a close relationship between tectonics and coda Q by comparing results from different regions in which Q has been studied by different authors using different or unknown parameters, for example, Woodgold (1994), Bianco *et al.* (1999), Zelt *et al.* (1999), Yun *et al.* (2007), Dobrynina (2011), and Farrokhi *et al.* (2015). However, because all the processing parameters are rarely, if ever, given, and different parameters can lead to different results, there might not be much substance to those claims. For example, none of the five references listed above present all the parameters used. Despite these uncertainties, it seems that coda Q values are related to both tectonic age and the amount of crustal heterogeneity (Sato *et al.*, 2012). It is not always clear, however, to what extent these differences are due to the processing parameters and how much are due to real coda Q differences.

Coda waves constitute the end of the seismic signal for the local and the regional events and the coda waves start after the S waves. Coda waves are composed of incoherent waves scattered by inhomogeneities and their amplitude is thought to decrease only due to attenuation (including scattering) and geometrical spreading. Aki and Chouet (1975) showed that, assuming that coda waves are single-scattered S waves at short source–receiver distances, the coda amplitude decay $A(f,t)$ as a function of frequency f and time t can be expressed as

$$A(f,t) = t^{-\beta} A_0 e^{\frac{-\pi f t}{Q_c(f)}}, \tag{1}$$

in which A_0 is the initial amplitude, β is the geometrical spreading parameter (1.0 for body waves, 0.75 for diffusion waves, and 0.5 for surface waves), and Q_c is coda Q. The geometrical spreading parameter is usually assumed to be 1.0 (e.g., Sato *et al.*, 2012) because the early part of the coda for local earthquakes is used. Taking logarithms and rearranging, equation (1) can be written as

$$\ln[A(f,t)] + \beta \ln(t) = \ln(A_0) - \frac{tf\pi}{Q_c(f)}. \tag{2}$$

*Now at Earthquake Administration of Shanxi Province, No. 69 Jinci Road, Taiyuan 030024, China.

Plotting the envelope of $\ln[A(f,t)] + \beta \ln(t)$ as a function of t for a given center frequency (by band-pass filtering the signal around the center frequency), gives a straight line with slope $-\pi f/Q_c(f)$ and $Q_c(f)$ can be determined by least squares. The envelope is obtained by calculating the root mean square (rms) values in a running window of a given length starting at a given time, the lapse time, and after the origin time. Alternatively, the envelope is sometimes calculated using the envelope definition with the Hilbert transform H (e.g., Farrokhi *et al.*, 2015) as

$$\text{Envelope}(f,t) = \sqrt{H[A(f,t)]^2 + A(f,t)^2}. \quad (3)$$

This method of using the coda Q decay envelope is called the coda wave decay (CWD) method and it is the most commonly used approach for determining coda Q, applied in many publications, both presently (e.g., Farrokhi *et al.*, 2015; Khan *et al.*, 2015; Singh *et al.*, 2015) and for the last 30 years (e.g., Zelt *et al.*, 1999; Bianco *et al.*, 2002; Mak *et al.*, 2004; Yun *et al.*, 2007; Mukhopadhyay *et al.*, 2008; Carcole and Sato, 2010; Rahimi *et al.*, 2010; Calvet and Margerin, 2013). Gusev (1995) in his review article provides many references up to 1994.

Coda Q (Q_c) is thought to consist of contributions from scattering and intrinsic Q:

$$Q_c^{-1} = Q_{sc}^{-1} + Q_i^{-1}, \quad (4)$$

in which Q_{sc} and Q_i are scattering and intrinsic Q, respectively. There are various interpretations of Q_c. Array analysis has shown that coda waves (particularly at high frequency) are dominated by S waves (Aki and Chouet, 1975; Sato *et al.*, 2012) so Q_c can be thought to represent Q_{sc} and Q_i of S waves. Several studies using different methods (see below) have tried to separate Q_i from Q_{sc}, sometimes with mixed results. Recent studies have been more consistent in finding that at short distances (0–100 km) Q_{sc} is dominant while at larger distances Q_i is dominant (e.g., Shapiro *et al.*, 2000). With a lapse time of 80 s, Bianco *et al.* (2002) found a close agreement between Q_c and Q_i. Mayeda *et al.* (1992) found that there was also a difference with respect to frequency for data at short distances. At frequencies <6 Hz, scattering was dominant, whereas intrinsic attenuation was dominant above 6 Hz.

All studies of coda Q find that there is an increase in attenuation with frequency as

$$Q_c = Q_0 (f/f_0)^{\alpha}, \quad (5)$$

in which Q_0 is Q at the reference frequency f_0 and α is a constant. Nearly all studies assume $f_0 = 1$ Hz such that the frequency dependence is fitted to

$$Q_c = Q_0 f^{\alpha}, \quad (6)$$

in which Q_0 is Q_c at 1 Hz. Thus, Q_0 and α are usually reported instead of the individual $Q_c(f)$ values.

There are other models for describing the coda decay than the simple single scattering theory that will give different Q-results, like multiple scattering and anisotropic scattering. For a more comprehensive overview, see Calvet and Margerin (2013).

The widely used coda normalization method (Aki, 1980; Sato *et al.* 2012) calculates Q of S waves using the spectral ratio of the S waves and coda waves. Examples are Ford *et al.* (2008) and Negi *et al.* (2015). Although using coda waves, the method is independent of the scattering model used for coda waves and the results are therefore not directly comparable with coda Q.

For regional earthquakes, the Lg coda waves are used. The Lg coda has less high-frequency content than the local coda waves at shorter distances, and the CWD method is therefore often not suitable at large lapse times due to lack of high-frequency content. Xie and Nuttli (1988) introduced the stacked spectral ratio method using a single trace. This method is frequently used for regional Lg coda Q studies (e.g., Mitchell *et al.*, 2015).

The multiple lapse-time window (MLTW) analysis introduced by Fehler *et al.* (1992) uses both S waves and coda waves to determine the intrinsic attenuation Q_i and the scattering attenuation Q_{sc} from which coda Q can be obtained. The logarithm of the integral of the energy in a time window is plotted against hypocentral distance and a number of time windows are used. The decay of energy with distance depends in different ways on intrinsic and scattering Q and by fitting the curves to a theoretical model, both intrinsic and scattering Q can be determined. Examples are Bianco *et al.* (2002) and Carcole and Sato (2010). The latter used both CWD and MLTW methods to determine Q in Japan.

The most important parameter in coda Q estimation is the lapse time (defined as the time lapsed after the origin time to where the coda Q analysis starts). Rautian and Khalturin (1978) observed amplitudes of band-pass-filtered seismograms for many different lapse times and found that coda amplitudes decay have a common shape at all the stations for windows starting mostly after about two times and always after three times the S-wave travel time. Therefore, most coda Q studies use a lapse time of at least twice the S-wave travel time. It is commonly observed that coda Q increases with lapse time, indicating that a single coda Q cannot be used to fit the whole coda wavetrain. This has been interpreted by many as an increase of coda Q with depth (e.g., Rautian and Khalturin, 1978; Ibáñez *et al.*, 1990). Gusev (1995) argued that the effect of scattering decreases with depth. He presented a model where the contribution of scattering to Q was proportional to h^{-n}, in which h is depth and n a constant. Using this model, he showed that the main differences between most published coda Q studies were simply due to using different lapse times. The differences in Q_c observed between studies using the same lapse time could then be due to other processing parameters being different or due to real difference in coda Q. Another explanation of increase in coda Q with lapse time is that the single scattering model might be too simple to

explain the coda decay. Calvet and Margerin (2013) found that, for events in the Pyrenees, the lapse time dependence could be explained by multiple anisotropic scattering without assuming any depth dependence of Q. Their data also show that Q_c does not increase infinitely with lapse time but reaches a constant level at a lapse time of 80–130 s. Their model of multiple anisotropic scattering fits with $Q_c = Q_i$ at long lapse times as also predicted by Shapiro *et al.* (2000).

Coda Q can thus be determined with different methods, all using several processing parameters, and the interpretation in terms of scattering and intrinsic Q will, to some degree, depend on the assumptions behind the methods. There is clearly a difference between results using local earthquakes (short lapse time) and regional earthquakes (long lapse time), and in general it is difficult to compare coda Q results from different studies unless the same methods and parameters are used, which is often not the case when using local earthquakes. This makes it difficult to evaluate how sensitive coda Q is to differences in tectonics. Others have also discussed these problems. For *Lg* coda Q studies, Mitchell *et al.* (2015) pointed out the importance of using the same procedures and parameters and claim to have done so in their many studies. For California, Ford *et al.* (2008) used five different methods, none of which was the CWD method, to determine *Lg* coda Q and found significant differences due to the varying methods, but also to the choice of parameters. Hellweg *et al.* (1995), in a study of California coda Q, also points out the importance of using the same parameters, in particular lapse time and length of analysis window, when comparing coda Q. In our study, we only use the CWD method to simplify the comparisons.

For an overview of the coda Q method as described above, see Havskov and Ottemöller (2010). The analysis presented here was performed using the SEISAN software (Havskov and Ottemöller, 1999).

In this study, we will first investigate the effect of using different processing parameters, select an optimal set of parameters, and then use the same computer program and the same (optimal) processing parameters to compare coda Q for local earthquakes for regions with supposedly different tectonics as well as similar tectonics. The regions are the Azores islands just off the mid-Atlantic ridge, Jan Mayen volcanic island near a transform fault of the mid-Atlantic ridge, continental southwestern Norway with nearby coastal areas, eastern Anatolia, Turkey, near the triple junction, the area around the Shanxi rift system, north China, and northwestern and central Argentina. These areas were selected because the authors had direct access to the data—which is particularly important for small local networks—and because the regions represent diverse tectonics. The purpose is to compare coda Q estimates to investigate how sensitive these values are to tectonic differences when differences due to processing parameters are ruled out. Only shallow events ($h < 35$ km) were considered in this study. This is done for two reasons: (1) we only want to compare shallow structures, since not all areas have deep events and events cannot be mixed because there is an indication that coda Q increases with depth, (2) using deep events, for example, at 200 km, would imply using much longer lapse times since the start of the coda analysis window must be at least twice the *S*-travel time and that would result in a too low signal-to-noise ratio (SNR) for many small shallow events.

Coda Q could also be affected by local soil conditions. Ibáñez *et al.* (1991) found an overestimation of coda Q at stations located on soil sites. This was interpreted as caused by reverberations in the soil layer. The coda decay curves also became irregular (lower correlations coefficient) at lower frequencies for stations near sedimentary basins. On the other hand, Steck *et al.* (1989) found higher coda Q with stronger frequency dependence for stations on rock sites compared with stations on soil sites, which they interpreted as an effect of filtering out the high-frequency coda waves in the sediments. Nearly all of our stations are on hard rock, so local soil conditions should be a minor problem even in the volcanic areas. Also, a test of using different ground-motion components (see later section) did not show any bias as one should have expected if there were serious site effects. Coda decay curves with strong irregularities will normally be discarded by the correlation threshold. That does not rule out site effects, but we consider it to be a minor problem for our data set.

Interpretation of the coda Q results in terms of scattering and intrinsic Q is not an exact science, as evidenced by the many often conflicting proposals (e.g., Frankel and Wennerberg, 1987; Bianco *et al.*, 2002; Carcole and Sato, 2010; Rachman *et al.*, 2015) and is out of scope for this study. We will also not try to compare coda Q estimates from our study with studies using other methods. The main purpose is to test the influence of processing parameters and get reliable coda Q estimates with the CWD method so results can easily be compared for different tectonic regions.

Data

For each region, events were selected which could potentially be used based on epicentral distance to the stations (< 100 km). A first coda Q test was then made and only the events which fulfilled the quality criteria, outlined in the next section, were selected. This reduced the available events by a factor up to 10. In the following, we only show the data actually contributing to the coda Q estimates. The stations and epicenters used for each area are shown in Figure 1.

The Azores Archipelago

The Azores archipelago (nine volcanic islands) is located on the Azores plateau at the triple junction where the North American, Nubian, and Eurasian lithospheric plates meet. The age of the islands is around 1 Ma (Johnson *et al.*, 1998; Calvert *et al.*, 2006). The area is seismically very active (Matias *et al.*, 2007) and there is significant volcanic activity (Silva *et al.*, 2012). Data from the Portuguese digital seismic network on the Azores (25 stations), currently operated by Instituto Português do Mar e da Atmosfera from

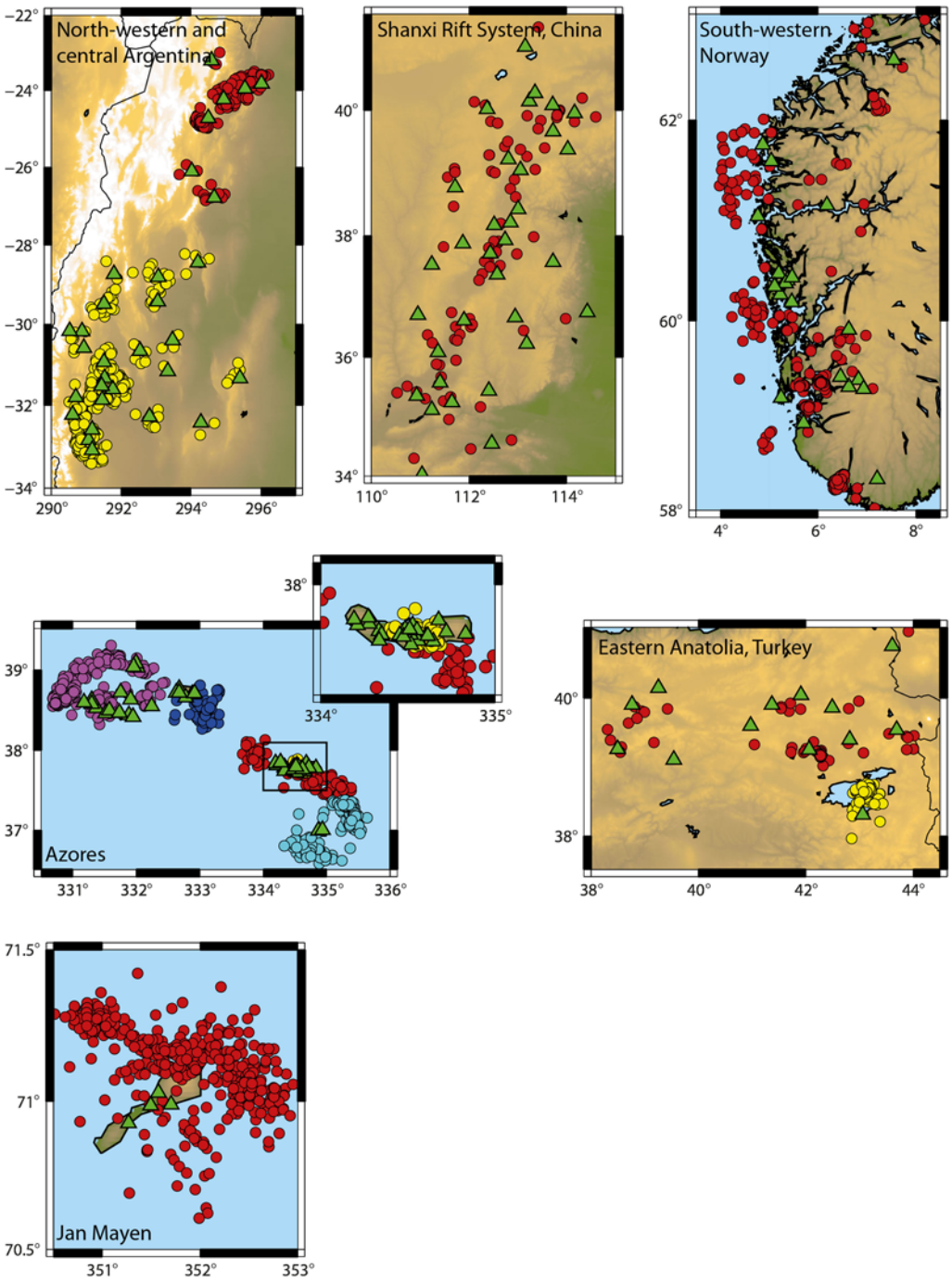

Figure 1. Study areas. The stations used are marked with triangles and the events with circles. For Argentina and eastern Anatolia, two groups were analyzed separately: north and south, and for the Azores there were five groups: west, middle, central, east, and a subset near the Fogo volcano (inset in figure for the Azores). Each group has different shading. The color version of this figure is available only in the electronic edition.

1996 to the present day, are used. A few events from the University of the Azores (used by the first author for another study, Silva *et al.*, 2012) were also used. Magnitudes were in the 0.6–6.1 range and the data covers the period 1998–2014. Many data are from analog stations with 12 bit resolution and 50 Hz sampling. The data from 1997 to 2007 were obtained in the framework of the former Sistema de Vigilância Sismológica dos Açores, a joint consortium between the Instituto de Meteorologia and the Centro de Vulcanologia e Avaliação de Riscos Geológicos.

Jan Mayen

Jan Mayen is a volcanic island located on the northern mid-Atlantic ridge between Greenland and Norway. It is situated just south of the Jan Mayen fracture zone, between the

two main spreading ridges in the North Atlantic. The area is seismically active with the occurrence of both volcanic and tectonic events (Havskov and Atakan, 1991). The oldest exposed lavas on the island are of upper Pleistocene age or around 1 Ma (Fitch *et al.*, 1965). A three-station digital seismic network, belonging to the Norwegian National Seismic Network, has been operational on the island since 1982 and a single broadband station after 2001. The data are mostly from the three station low dynamic range (12 bit, 50 Hz sampling) network with short-period sensors, of which one has three components. Magnitudes are in the range 1.1–5.8 and the data cover the period 1983–2015.

Southwestern Norway

Southwestern Norway represents a stable continental region with low-to-moderate seismicity. Most seismicity is located offshore in a belt along the west coast of the Norwegian mainland. The basement in the area is mainly pre-Cambrian with some parts of Cambrian–Silurian age (Torske, 1977). The Norwegian National Seismic Network is currently operating 14 seismic stations in this area, some are broadband and some are short period. For the early part of the data, most are short period with 50 Hz sampling. Magnitudes are in the 0.8–3.6 range and the data cover the period 1985–2015.

The Shanxi Rift System

The Shanxi Rift System is located in north China. The present rift system has formed mainly since Pliocene (Xu *et al.*, 1993) as a result of the far-field effect of the India–Eurasia collision. The area was mainly formed around 2000 Ma ago (Chen *et al.*, 2012). The rift system is seismically highly active. Instrumental seismic monitoring has taken place since 1970 (Wu, 1982). The regional network operated by the Shanxi Seismic Network Center currently has 56 broadband stations, covering an area of about 250 km × 650 km (Li *et al.*, 2015). Sample rate is 100 Hz. Magnitudes are in the range 2.4–4.4 and the data cover the period 2009–2014.

Argentina

Argentina is tectonically dominated by eastward subduction of the oceanic Nazca plate beneath the South American continental plate. The resulting shallow seismicity is concentrated in the central and northwestern parts of the country, along the Andean back-arc region (Richardson *et al.*, 2012). The area of shallow seismicity in the back-arc of the Andes is at least of Cambrian age (Vujovich *et al.*, 2004). The seismically active area is monitored by the National Seismic Network of 46 stations, both short period and broadband, operated by National Institute for Seismic Prevention (Sanchez *et al.*, 2013). Some are low sample rate (40 Hz) and 12 bit resolution. Magnitudes are in the 0.4–6.1 range and the data cover the period 2009–2012.

Eastern Anatolia

Eastern Anatolia is tectonically mainly controlled by the collision of the Arabian plate with Eurasia. This causes the Anatolian microplate to be pushed westward, and the buildup of the East Anatolian plateau (Reilinger *et al.*, 1997). The crust of eastern Anatolia is relatively young (50–100 Ma, Boztuğ and Harlavan, 2008) with active volcanism (Aydar *et al.*, 2003). The East Anatolian plateau is associated with a high level of seismicity distributed on numerous small fault systems. The region is monitored by the Atatürk University seismic network consisting of eight stations owned by the Atatürk University, 16 stations owned by the national network (AFAD) based in Ankara, and two stations from Georgia. All stations are broadband with 100 Hz sample rate. Magnitudes are in the 1.1–5.3 range and the data cover the period 2011–2012.

Our study areas, as outlined above, comprise two areas with very young volcanic islands (Azores and Jan Mayen), three areas of old crust (Norway, Argentina, and the Shanxi rift system), and one younger area with active volcanism (eastern Anatolia). This should provide a good basis for comparison of the results from the coda Q analysis.

Coda Q Parameters

In the following, we will describe in detail the parameters used for determining coda Q and test the influence of some of the parameters on the results. All data from different regions were used and showed comparable variation in the results as a function of the parameters. Based on the tests, final parameters for processing are selected. For each test, we compare its results with the results of our final selection of parameters, the reference parameters. For the tests, we present only the results for the data from the Shanxi rift system (see below), except for a set of very different parameters where all areas are used. The data from the Shanxi rift system are from a homogeneous high-quality three-component broadband network and therefore is good for testing.

For a given data set, average coda Q values at each frequency were calculated based on all recordings fulfilling the given selection criteria. The averages were calculated using the $1/Q$ values. An alternative approach, followed by some authors, is to do a least squares inversion for all envelopes simultaneously, which can also calculate the geometrical spreading parameter (Aki and Chouet, 1975). However, this is equivalent to our approach as also tested by Kvamme and Havskov (1989). Finally, for each data set, the average coda Q values were fitted to the relation $Q = Q_0 f^{\alpha}$. Each value was weighted with the number of Q-values used for calculating the average at that frequency.

The number of successful Q-determinations at any frequency and component and Q_0 and α is determined and compared for the different tests. Q at 10 Hz is also calculated because it is not always easy to compare the $Q(f)$ relations and we find that difference in Q is particularly noticed at higher frequencies. The parameters considered best were

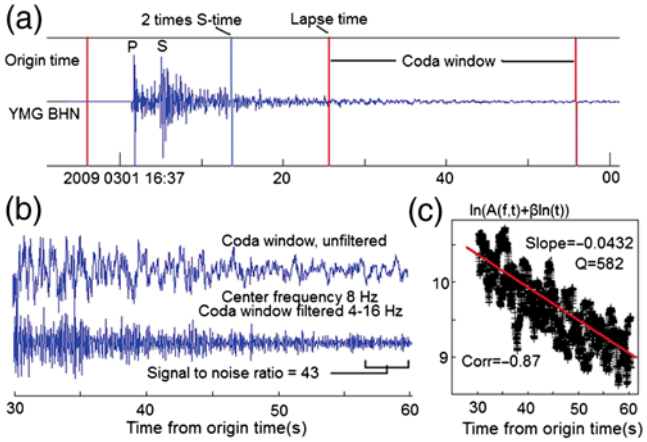

Figure 2. Coda wave processing. (a) The trace shows the original unfiltered trace with the coda window position selected. It is seen that the lapse time (time from origin to start of coda window) is larger than twice the *S*-travel time. (b) The filtered and unfiltered coda decay window. It has a good signal-to-noise ratio (SNR) of 43 measured as indicted for the last 3 s of the filtered window. (c) The corrected coda envelope as a function of time. The correlation coefficient of the fit is 0.87 and the slope is 0.0432 giving a coda Q of 582. The data are from the Chinese data set for channel YMG BHN for event with origin time 2009 0301 16:36 56.0. The color version of this figure is available only in the electronic edition.

selected mainly based on the number of good fits to the decay curve and partly on the best fit to equation (6). Figure 2 gives an example and illustrates some of the parameters used.

Components to Use

Because coda waves are random and coming from all directions, we would not expect any difference between the components. This was also observed by Del Pezzo *et al.* (1985) and Sato *et al.* (2012) and to use more observations, all three components should be used. Table 1 shows the results using individual components and all three components, and the results are almost identical. This also indicates the stability of the CWD method. We use all three components where available.

The Geometrical Spreading Parameter β

The geometrical spreading parameter β is usually fixed to 1.0 for body waves. However, when both Q and the geometrical spreading parameter are determined, there is a coupling between the two. Aki and Chouet (1975) point out that the results are relatively insensitive to β. Rautian and Khalturin (1978) mention that different β-values of 0.5–1.0 affect the result by less than 20%. Calvet and Margerin (2013) found 10% difference between using 0.75 and 1.0. They used 0.75 since, in their approach, coda waves were interpreted using multiple scattering converging toward diffusion. Bianco *et al.* (1999) assumed surface waves and used $\beta = 0.5$ for a local study (lapse times 8–12 s) of Vesuvius. We tested with the three different spreading parameters. It is seen that the obtained Q-values are affected by up to 20% by the spreading parameter (Table 2). However, the fit seems better for spreading parameter 0.5 than for 1.0 and 0.75 as indicated by the larger number of acceptable results. This could be due to the lowest frequencies representing surface waves. Rautian and Khalturin (1978) found that $\beta = 0.5$ gave a slightly better fit to the data for the lowest frequencies interpreting this as the lowest-frequency coda waves were representing surface waves. However, other studies have found a higher value of β. Ibáñez *et al.* (1993) found a value of $\beta = 1.2$ using coda waves independently of determining coda Q. For *Lg* waves, Akinci *et al.* (1995) found β values between 0.5 and 0.9 by inverting their data set for Q and β simultaneously. The epicentral distances were 100–400 km so their results are not directly comparable to our study with distances <100 km. They do, however, illustrate that geometrical spreading might not be what we expect. Vidales-Basurto *et al.* (2014) studied *S*-wave attenuation in the region of the Gulf of California. For distances of 10–120 km, the β-values were 0.8–1.0 and for 120–220 km they found β-values of 0.4–0.7. Using array observations for events at 10–150 km distances, Akinci *et al.* (2014) studied high-frequency attenuation in Turkey and found that $\beta = 1.0$ for distances <40 km and $\beta = 0.3$ for distances >40 km. In our study, we would have expected a value near 1.0, as also found in studies where Q and geometrical spreading have been determined simultaneously. Galluzzo *et al.* (2015) found that above 6 Hz, the coda waves were pure body waves, whereas below 6 Hz they were a mixture of surface and body waves. Thus, the geometrical spreading parameter could be less than 1 for lower frequencies.

As illustrated above, there is quite a range of β-values used or observed, which might depend on both the distance and frequency range considered. In our study, we cannot claim to find the correct geometrical spreading, but we have found the single value that best fits the data. It might then be

Table 1
Coda Q for Different Components

Component	NT	Q_0	α	Q_{10}
Z, N, E reference	1407	99 ± 3	0.89 ± 2	763 ± 23
Z	451	100 ± 4	0.88 ± 2	766 ± 30
N	476	99 ± 4	0.88 ± 2	760 ± 30
E	480	97 ± 3	0.90 ± 2	764 ± 24

NT, the total number of coda Q determinations at any frequency; Q_{10}, Q at 10 Hz. Errors shown are standard deviation; Z, vertical; N, north; and E, east.

Table 2
Test with Different Spreading Parameters

Spreading Parameter	NT	Q_0	α	Q_{10}
0.5 reference	1407	99 ± 4	0.89 ± 2	763 ± 31
0.75	1147	114 ± 5	0.88 ± 2	876 ± 38
1.0	1138	131 ± 5	0.88 ± 3	988 ± 38

NT, the total number of coda Q determinations at any frequency; Q_{10}, Q at 10 Hz. Errors shown are standard deviation.

Table 3
Tests of Different Bandwidths

Bandwidth (octaves)	Number of Poles	n	Q_0	α	Q_{10}
2.0 reference	8	1407	99 ± 4	0.89 ± 0.02	763 ± 31
0.5	8	1062	78 ± 3	0.95 ± 0.02	694 ± 27
1.0	8	1306	92 ± 5	0.91 ± 0.03	742 ± 41
1.2	8	1365	96 ± 5	0.89 ± 0.03	750 ± 39
1.5	8	1379	98 ± 5	0.89 ± 0.02	754 ± 39
3.0	8	1409	99 ± 3	0.89 ± 0.01	773 ± 23
2.0	4	1439	99 ± 3	0.89 ± 0.02	764 ± 23

NT, the total number of coda Q determinations at any frequency; Q_{10}, Q at 10 Hz. All tests are with an eight-pole filter, except the last which is with a four-pole filter. Errors shown are standard deviation.

Table 4
Coda Q as a Function of Lapse Time and Window Length

Lapse Time (s)	Window (s)	NT	Q_0	α	Q_{10}
30	30	1407	99 ± 4	0.89 ± 0.02	763 ± 31
Reference	Reference				
20	30	1340	80 ± 2	0.91 ± 0.02	654 ± 16
40	30	1946	127 ± 10	0.86 ± 0.03	917 ± 73
50	30	2127	151 ± 17	0.84 ± 0.05	1038 ± 118
30	40	1375	117 ± 4	0.86 ± 0.07	847 ± 29
30	50	1302	139 ± 7	0.82 ± 0.03	925 ± 46
40	20	1586	101 ± 5	0.89 ± 2	776 ± 39
50	20	1537	109 ± 7	0.90 ± 4	865 ± 56
60	20	1336	114 ± 10	0.89 ± 4	883 ± 78

NT, the total number of coda Q determinations at any frequency; Q_{10}, Q at 10 Hz. Errors shown are standard deviation.

that the low value is caused by an imperfect scattering model or by a frequency dependent mixture of body and surface waves. However, it is beyond the scope of our study to investigate that. We therefore choose to use $\beta = 0.5$ for our optimal set of processing parameters but present also the results obtained using $\beta = 1.0$.

Signal Filtering

The geometric center frequencies, representing the energy in a filter, were 1, 2, 4, 8, and 16 Hz. The geometric center frequency f_c, is calculated as $f_c = \sqrt{(f_u \times f_l)}$, in which f_u and f_l are higher and lower cutoff frequencies, respectively. The filter width is often one octave, but other filter bands are also used. Choosing a too narrowband might result in rapid changes in the filtered coda envelope which then becomes unstable (Sato *et al.*, 2012), resulting in a bad fit of the envelope. A too wide filter might blur the distinction between the different frequencies. Tests were made with different bandwidths, as presented in Table 3.

It is seen that the filter width influences the results with an increase in Q_0 for increasing filter width, becoming stable when using a 1.5 octave filter. A wider filter also results in more acceptable results and at the same time a better fit to the $Q(f)$ curve. We therefore use a two octave filter giving the following bandwidths (Hz): 0.5–2.0, 1–4, 2–8, 4–16, and 8–32. Two octaves are more than is used in most studies. Some of the data was sampled at 40–50 Hz so the higher band could not be used for those events. The filter used is an eight-pole Butterworth filter with zero phase shift. Most studies use four- or eight-pole filters. As seen from Table 3, it makes no significant difference if using four or eight poles.

Lapse Time

The lapse time is from the origin time to the start of the coda window used. Some studies define it as the time from the origin to the middle of the analysis window. The lapse time is often set to twice the *S*-travel time, but that is a bad practice since the lapse time in that case will be dependent on the data set and different for each event. It will thus be impossible to compare with other data sets. When comparing data from different areas with different attenuation and sizes of earthquakes, it is important to find a common lapse time. For an area like Jan Mayen, large lapse times cannot be used due to the small magnitudes of events and low SNR. For the areas compared in this study, which have both very low and high Q-areas, a lapse time of 30 s was a good compromise to get enough results. This corresponds to a hypocentral distance of up to about 60 km. It also means that the coda Q determinations are not representative of *Lg* which usually starts at 150–200 km. Table 4 shows the dependence on lapse time. It is seen that there is a clear increase in Q with lapse time for a 30 s window length (as expected). We also show lapse time dependence for a 20 s window where it is seen that the increase of Q with lapse time is not very pronounced. This will be discussed further in the next section.

The Window Length for Analysis

The window length for analysis selected for the coda Q processing affects the results as this implies sampling of different volumes like the lapse time. A longer window would therefore be expected to give larger Q-values as we also observe (Table 4). The window selected should be long enough to produce a stable envelope. In practice, 20–30 s are often used. In our study, we tried using 20 s to get the maximum use of the low SNR data from the volcanic areas. However, we got more acceptable results with 30 s indicating it might be better. One would expect a 50 s window with a lapse time of 30 s to give a result comparable with or a bit smaller than for a 30 s window with a lapse time of 50 s since both have the same end of the coda window (80 s from the origin). This is also what is observed indicating that the single scattering model with the parameters used here fits the data quite well. The same test was made with a 20 s window where we would expect a lapse time of 60 s to give a similar result as a window of 30 s and a lapse time of 50 s. However when using a 20 s window, Q increases less than expected with increasing lapse time, indicating that a 20 s window is too short to get stable results. We therefore selected a 30 s window. Using a 30 s window instead of 20 s has the implication that a larger area

Table 5
Coda Q as a Function of Minimum Lapse Time

Start in S Times	NT	Q_0	α	Q_{10}
2.0 reference	1407	99 ± 4	0.89 ± 2	763 ± 31
1.5	2438	100 ± 3	0.87 ± 2	749 ± 22
2.5	830	99 ± 4	0.88 ± 2	752 ± 30

NT, the total number of coda Q determinations at any frequency; Q_{10}, Q at 10 Hz. Errors shown are standard deviation.

Table 6
Influence of Root Mean Square (rms) Window Length

rms Window Length	n	Q_0	α	Q_{10}
5 cycles reference	1407	99 ± 4	0.89 ± 2	763 ± 31
3 cycles	1382	95 ± 3	0.90 ± 2	754 ± 24
7 cycles	1369	103 ± 4	0.87 ± 2	769 ± 30
Fixed 3 s	1358	96 ± 3	0.92 ± 2	800 ± 25
Fixed 5 s	1358	101 ± 3	0.91 ± 2	819 ± 24

NT, the total number of coda Q determinations at any frequency; Q_{10}, Q at 10 Hz. Errors shown are standard deviation.

is sampled and it will be more difficult to see small regional contrasts in coda Q.

Minimum Lapse Time

Minimum lapse time is often set to twice the S-travel time but could be more since it is considered that coda waves only start at that time. This means that if the lapse time is less than twice the S-time, the event is rejected. The S-time is taken from the S-reading, if no S-reading is available; the P-reading is used to calculate the S-arrival time. If no phase reading is available, the station is not used. Our tests showed that the minimum time was not critical for the results (Table 5), and using a smaller minimum time gave more results since more events would also fulfill the requirement of absolute lapse time start of 30 s. Because a value of 1.5 gave nearly the same result as 2.0, it could indicate that in our test data, the coda waves are dominant already at 1.5 times the S-time. However, the generally accepted twice the S-time is used. Mukhopadhyay and Sharma (2010) tested with the same values and found similar results.

The Length of the rms Window

The coda envelope is calculated as the rms of the filtered signal using a sliding window which is five cycles long. This value is normally never changed. Other studies use a fixed rms window (e.g., Farrokhi *et al.*, 2015) of 2–5 s. It should be long enough to smooth out the envelope but not so long as to completely ruin the shape of the envelope. Tests were made with three and seven cycles as well as fixed lengths (Table 6) and it can be observed that the length of the rms window affects Q_0 but less so Q_{10}. We see no obvious reason to change the rms length and continue to use five cycles.

Table 7
Influence of Signal-to-Noise Ratio (SNR)

Signal-to-Noise Ratio	NT	Q_0	α	Q_{10}
3 reference	1407	99 ± 4	0.89 ± 2	763 ± 31
2 and 3 s window	1483	99 ± 3	0.89 ± 2	763 ± 23
4 and 3 s window	1315	99 ± 4	0.89 ± 2	763 ± 31
3 and a 5 s window	1421	99 ± 4	0.89 ± 2	763 ± 31

NT, the total number of coda Q determinations at any frequency; Q_{10}, Q at 10 Hz. Errors shown are standard deviation.

Table 8
Influence of Maximum Correlation Coefficient

Maximum Correlation Coefficient	NT	Q_0	α	Q_{10}
−0.6 reference	1407	99 ± 4	0.89 ± 2	763 ± 31
−0.5	1456	102 ± 4	0.88 ± 2	769 ± 30
−0.7	1306	96 ± 3	0.89 ± 2	750 ± 23
−0.8	960	92 ± 3	0,89 ± 2	703 ± 23
−0.9	230	80 ± 2	0.88 ± 2	612 ± 15

NT, the total number of coda Q determinations at any frequency; Q_{10}, Q at 10 Hz. Errors shown are standard deviation.

The Signal-to-Noise Ratio

The SNR is calculated as the ratio between a given number of seconds of the rms amplitude at the end of the filtered signal and the same length window in the noise before the event (Fig. 2). We use a 3 s window and a SNR of three. Using SNRs of two and four gives almost the same result, as does using a 5 s window (Table 7). These parameters are not critical.

The Maximum Correlation Coefficient

Log of the decay curve is fitted with a line by least squares and the correlation coefficient is calculated. Only data with a negative correlation coefficient smaller than a given value are used. This value is a trade-off between getting enough Q-determinations and a high-quality fit as seen in Table 8. It is also seen that the choice of value significantly affects the Q_0-values. We use −0.6 as a compromise.

Other Criteria

Coda Q values smaller than 10 and larger than 10,000 were rejected. The data had both 12 and 24 bit resolution and it was automatically checked for clipping and clipped data were rejected.

Based on the parameter testing, we recommend the following set of optimal parameters for coda Q analysis using the CWD method:

- Geometrical spreading parameter, β: 0.5
- Filter: two octave-wide Butterworth filter with eight poles and zero phase shift
- Lapse time: 30 s

Table 9
Comparing Several Parameters at the Same Time

	Bandwidth = 2			Bandwidth = 1		
	NT	Q_0	Q_{10}	NT	Q_0	Q_{10}
$\beta = 0.5$						
$W = 20$	1345	80 ± 2	655 ± 20	1103	68 ± 3	613 ± 25
$W = 30$	1407	99 ± 4	763 ± 31	1306	92 ± 5	742 ± 41
$\beta = 0.75$						
$W = 20$	1173	89 ± 3	722 ± 28	881	72 ± 3	657 ± 27
$W = 30$	1334	114 ± 5	876 ± 36	1156	100 ± 6	830 ± 48
$\beta = 1.0$						
$W = 20$	923	97 ± 3	789 ± 28	643	75 ± 3	694 ± 24
$W = 30$	1138	131 ± 5	988 ± 38	921	109 ± 7	917 ± 56

β, geometrical spreading; W, window length (s), and bandwidth is the number of octaves in the filter. NT, the total number of coda Q determinations at any frequency; Q_{10}, Q at 10 Hz. Errors shown are standard deviation.

- Window length: 30 s
- Length of rms window: five cycles
- Minimum SNR: 3
- Maximum correlation coefficient: −0.6

When many parameters are tested one at a time, there might be a combination effect not seen. We have therefore made a combination test of the parameters mostly affecting the results, as presented in Table 9. As observed, the largest number of good fits is obtained when using our recommended parameters: window length 30 s, geometrical spreading 0.5, and a two octave filter. Just changing these parameters, which are all within a reasonable range, the Q_0-values change by almost a factor 2 while the Q_{10}-values change by up to a factor 1.6.

In most studies, only some of the above parameters are reported. It is well known that the lapse time and window length have a strong influence on the results but less so with filter width, length of rms window, and correlation coefficient. Filter width, length of rms window, and correlation coefficient have significant effect on Q_0 but little effect on Q_{10} indicating that the variation is purely a processing effect. Thus, the true Q_0 might be more difficult to determine than the true Q_{10}. By choosing the right parameters, almost any coda Q can be obtained, and it should be clear that without using the same parameters for at least the critical parameters, comparison of coda Q values from different studies is not possible. Our final parameters are different from what other coda Q studies have been using in terms of filter width and geometrical spreading and we will therefore later also compare our results with what is obtained with traditional parameters.

Coda Q for Different Tectonic Areas

The coda Q results for all the study areas are presented in Tables 10 and 11 and Figure 3. Results for the individual regions will be described in the following.

The Azores Archipelago

On the Azores, the area around the Fogo volcano on S. Miguel is known to have a low Q (D. Silveira, personal comm., 2010) and the data around Fogo was therefore treated separately. Coda Q was calculated separately for the four island groups, where the central group with Fogo did not have the Fogo events included (Fig. 1, the different groups are indicated with different colors). The Fogo events were required to have an epicentral distance < 20 km to the volcano. No significant differences were found between these groups and all data were therefore grouped together. For the central west area, Carvalho *et al.* (2015) did a coda Q study using geometrical spreading parameter 1.0, window length 20 s and lapse time at two times the S-travel time and got $Q = 76f^{0.69}$. The parameters are almost the same as our alternative parameters and the Q-relation also nearly the same. An earlier unpublished study (D. Silveira, personal comm., 2010) used substantially more data than our study, particularly in the Fogo area. Using a 20 s window, lapse time 30 s, geometrical spreading 1, 0.8 octave bandwidth, and five cycle rms averaging she got $Q = 62f^{0.85}$ for all islands and $Q = 60f^{0.64}$ for Fogo. These closely match the estimates found in our study when using almost the same parameters (Table 10) but are smaller than the Q-values obtained with our preferred parameters. However, both studies show a clear difference in Q between Fogo area and the rest of the Azores.

Jan Mayen

The small Jan Mayen network does not allow for any coda Q calculation in different areas and the SNR is quite low so there were not as many results as for the Azores. In a previous study, Havskov *et al.* (1986) determined an average $Q = 113f^{0.46}$ using a small data set (20 Q determinations from seven events). Lapse time was twice the S-time, window length 15–25 s, geometrical spreading 1.0 and rms averaging over five cycles so parameters are different to our study. Consequently, coda Q is quite different from the results of our study with coda Q higher at low frequencies and

Table 10
Coda Q Values in Different Regions

Region	NT	Nev	nst	Q_0	α	Q at 1.5 Hz	Q at 10 Hz
Azores	7671	864	34	86 ± 5	0.70 ± 0.04	114 ± 7	429 ± 25
West	5383	535	16	88 ± 4	0.68 ± 0.04	116 ± 5	418 ± 19
Middle	589	63	8	76 ± 2	0.71 ± 0.02	101 ± 3	386 ± 10
Central	739	100	12	92 ± 6	0.72 ± 0.06	123 ± 8	485 ± 31
South	960	166	2	79 ± 8	0.79 ± 0.08	108 ± 11	483 ± 50
Alt	8587	989	38	79 ± 4	0.74 ± 0.03	107 ± 5	439 ± 22
Fogo	485	68	18	69 ± 2	0,64 ± 0.04	90 ± 3	302 ± 9
Alt	554	77	17	77 ± 4	0.45 ± 0.06	92 ± 5	218 ± 11
Jan Mayen	3073	448	4	90 ± 5	0.72 ± 0.04	121 ± 7	469 ± 26
Alt	2844	589	4	77 ± 5	0.80 ± 0.05	106 ± 7	483 ± 32
Norway	1771	3480	20	124 ± 7	0.91 ± 0.03	179 ± 10	997 ± 57
Alt	415	229	15	85 ± 1	0.97 ± 0.01	110 ± 2	760 ± 9
Argentina	2212	539	45	89 ± 4	0.94 ± 0.03	131 ± 6	773 ± 35
North	895	227	11	80 ± 1	0.97 ± 0.01	119 ± 2	749 ± 9
South	1317	312	34	105 ± 8	0.87 ± 0.0 4	149 ± 11	772 ± 59
Alt	1022	477	46	66 ± 4	1.05 ± 0.04	101 ± 6	733 ± 45
Turkey	1078	162	13	88 ± 4	0.66 ± 0.04	115 ± 5	402 ± 18
South	733	103	1	87 ± 4	0.67 ± 0.03	115 ± 5	409 ± 19
North	345	59	12	89 ± 5	0.64 ± 0.05	115 ± 6	385 ± 22
Alt	617	111	12	81 ± 3	0.67 ± 0.02	106 ± 4	380 ± 14
China	1407	80	34	99 ± 4	0.89 ± 0.02	142 ± 6	763 ± 31
Alt	643	73	31	76 ± 3	0.96 ± 0.02	112 ± 4	695 ± 27

NT, the total number of coda Q determinations at any frequency; Nev, number of events; nst, number of stations; Q_0 and α, the parameters in the $Q(f)$) relation. Under Region, the entry Alt is determination with three alternative parameters for the main area, window length is 20 s, geometrical spreading is 1.0 and a one octave filter. Errors shown are standard deviation.

lower at high frequencies (Q_{10} in the previous study and current study are 326 and 469, respectively). However, the earlier results are based on very few data.

Southwestern Norway

All of southwestern Norway, including offshore areas, was selected. This means that parts of the ray paths are below the North Sea because many events are offshore. No tests were made for different areas. The only earlier results (Kvamme and Havskov, 1989) with some stations and events also in eastern Norway gave $Q = 75f^{1.15}$. The window length was 30 s, but there was no control of lapse time since two times the S time was used. Epicentral distances were in the 20–150 km range so average lapse times might be a bit longer than in our study. The other parameters were geometrical spreading 1.0, filter width around 1.2 octave, and a five cycle rms averaging. Their Q_{10} (1060) is comparable with our study ($Q_{10} = 997$) while we get a higher $Q_0 = 124$, most likely due to the other processing parameters being different.

Eastern Anatolia

For this area in eastern Anatolia, it is seen that there is a large number of aftershocks of the 2011 Van earthquake (Fig. 1) so these were studied in one group (south) and the rest in another group (north). The results were almost identical so the final coda Q estimates are given for the whole area. For an area (36–40 °N, 36–41 °E) partly overlapping with our area, Sertcelik (2012) also determined coda Q using data from the Kandilli Observatory and Earthquake Research Institute. For a lapse time twice the S time, window length of 30 s, geometrical spreading of 1.0 and 1 octave bandwidth, minimum SNR of five and minimum correlation coefficient of 0.85, the average result was $Q = 60f^{0.82}$ ($Q_{10} = 396$). This is close to our results for Q_{10}, but a bit lower for Q_0, partly due to different parameters. However, both studies confirm a relatively low Q for this area.

Northwestern and Central Argentina

The data used are from the northwest and central part of the country where the most important shallow intraplate activity takes place and no data from the Chilean shallow subduction zone was included. Separate analysis was made for the two areas (north and south). There was a small difference in coda Q_0 between these two areas but not much for Q_{10}. Because the difference was small, the two groups were merged. Badi *et al.* (2009) studied Q from both shallow and deep events in the southern part of our study area using different methods, among these CWD. For shallow events, they found approximately $Q_0 = 100$ and $Q_{10} = 1300$ while we found values of 149 and 772, respectively. Few parameters were given by Badi *et al.* (2009); however, the lapse time was 90 s, substantially longer than the 30 s we use, and one could therefore expect a higher Q as also observed for Q_{10}.

Table 11
Details of Coda Q Results for Each Region

	1			2			4			8			16		
Frequency (Hz)	NT	$Q \pm$ std. dev.	Corr	NT	$Q \pm$ std. dev.	Corr	NT	$Q \pm$ std. dev.	Corr	NT	$Q \pm$ std. dev.		NT	$Q \pm$ std. dev.	Corr
Azores	1844	91 ± 28	0.88	2591	134 ± 31	0.86	2157	217 ± 47	0.84	980	394 ± 93	0.86	99	723 ± 214	0.82
Alt	850	83 ± 32	0.77	2432	134 ± 40	0.76	2587	211 ± 55	0.78	1409	380 ± 120	0.77	349	691 ± 227	0.76
Fogo	186	69 ± 22	0.88	207	110 ± 33	0.86	80	160 ± 53	0.84	12	292 ± 99	0.78			
Alt	163	76 ± 35	0.78	287	109 ± 33	0.79	84	129 ± 53	0.81	17	220 ± 58	0.77	3	397 ± 19	0.70
Jan Mayen	796	95 ± 28	0.85	1002	143 ± 33	0.85	822	230 ± 49	0.85	369	440 ± 111	0.82	84	697 ± 111	0.88
Alt	378	85 ± 35	0.77	1016	131 ± 38	0.77	933	220 ± 54	0.76	343	424 ± 124	0.73	174	790 ± 175	0.76
SW Norway	34	105 ± 59	0.78	113	230 ± 111	0.74	498	441 ± 135	0.75	805	862 ± 176	0.75	321	1470 ± 279	0.75
Alt	36	31 ± 32	0.77	53	150 ± 70	0.72	113	298 ± 121	0.70	124	605 ± 141	0.67	86	1204 ± 302	0.65
Argentina	304	83 ± 33	0.85	467	175 ± 70	0.83	608	344 ± 110	0.83	686	617 ± 108	0.85	147	1122 ± 190	0.80
Alt	210	69 ± 29	0.81	218	126 ± 53	0.76	204	276 ± 97	0.72	314	612 ± 119	0.68	76	1101 ± 190	0.67
E Anatolia	226	93 ± 29	0.83	292	133 ± 28	0.83	330	213 ± 37	0.78	207	358 ± 60	0.78	23	634 ± 192	0.77
Alt	123	85 ± 29	0.77	177	125 ± 37	0.76	185	202 ± 50	0.75	102	338 ± 70	0.73	30	532 ± 122	0.72
Shanxi rift	200	101 ± 30	0.84	228	172 ± 38	0.85	269	344 ± 69	0.84	345	644 ± 122	0.82	365	1139 ± 198	0.80
Alt	112	78 ± 29	0.79	140	140 ± 44	0.75	96	294 ± 68	0.72	130	576 ± 107	0.69	165	1081 ± 189	0.68

T, the total number of coda Q determinations at given frequency; std. dev., standard deviation in average; corr, average correlation for determining Q for each decay curve at the given frequency. Alt means Q-determinations with alternative parameters: window = 20 s; geometrical spreading = 1.0 and a one octave filter. Note that there are no results for Fogo when using a two octave filter since many stations in the area have 50 Hz sample rate. Errors shown are standard deviation.

The Shanxi Rift System

There was no obvious division to make in the Shanxi rift system and due to the relatively large distance between stations in the network, only a few results were obtained when using a lapse time of 30 s and all data were grouped together. Three studies have used earlier data from the network. All three used a lapse time of twice the S time. For the northern part of the rift system, Jin *et al.* (2012) used a window length of 40 s and got an average for 12 stations of $Q = 28f^{0.96}$. Jin *et al.* (2008) used data from one station, also in the northern part of the rift system, and for a window length of 30 s got $Q = 29f^{0.90}$. Both these studies gave much smaller Q than found in our study. Ning *et al.* (2012) used data from the whole area but with a window length of 80 s. The average result for 13 stations was $Q = 166f^{0.61}$. Because of the long time window, a much larger Q_0 was obtained. These three studies are clearly not comparable with our results due to different parameters used and maybe also due to different ways of processing.

Comparing results for our test areas with earlier published results, it is seen that when parameters are close, the results are also similar.

Discussion

Comparing coda Q values for the different tectonic regions (Tables 10 and 11 and Fig. 3), it can be observed that there is up to a factor 2 difference of Q_0 whereas at 10 Hz there is up to a factor 3 difference. In Figure 4, we illustrate this by making a histogram of the individual Q-values for each region. The figure shows that despite the relatively large scatter in the data, there is a clear difference in coda Q between some regions and a clear similarity between others. A similar observation was made by Bianco *et al.* (2002) who also found that the difference in coda Q between different areas was most pronounced at high frequencies.

According to Gusev (1995) (Fig. 5), the average global results at a lapse time of 30 s (in accordance with his prediction) at 1.5 Hz is $Q = 80$ (his parameter $n = 3$) to 120 ($n = 2$), whereas the corresponding observations he uses are in the 60–130 range. Our results with the recommended optimal parameters give a larger range of 90–179. If we use the alternative parameter set, the range is only 92–112 which again illustrates the importance of processing parameters. It might also indicate that the results are less reliable with the alternative parameters. Gusev (1995) also compiled α as a function of lapse time and found a decrease of α from 1.0 to 0.6 in the lapse time range 10–100 s. At 30 s, the observations were in the range 0.7–1.1 and ours are in the range 0.6–1.1, which is quite similar.

Using the alternative parameters, there are much fewer results. The average correlation coefficients are also systematically lower indicating a worse fit to the coda decay model. Above we also found that using a 20 s window, there was no good correspondence between window length and lapse

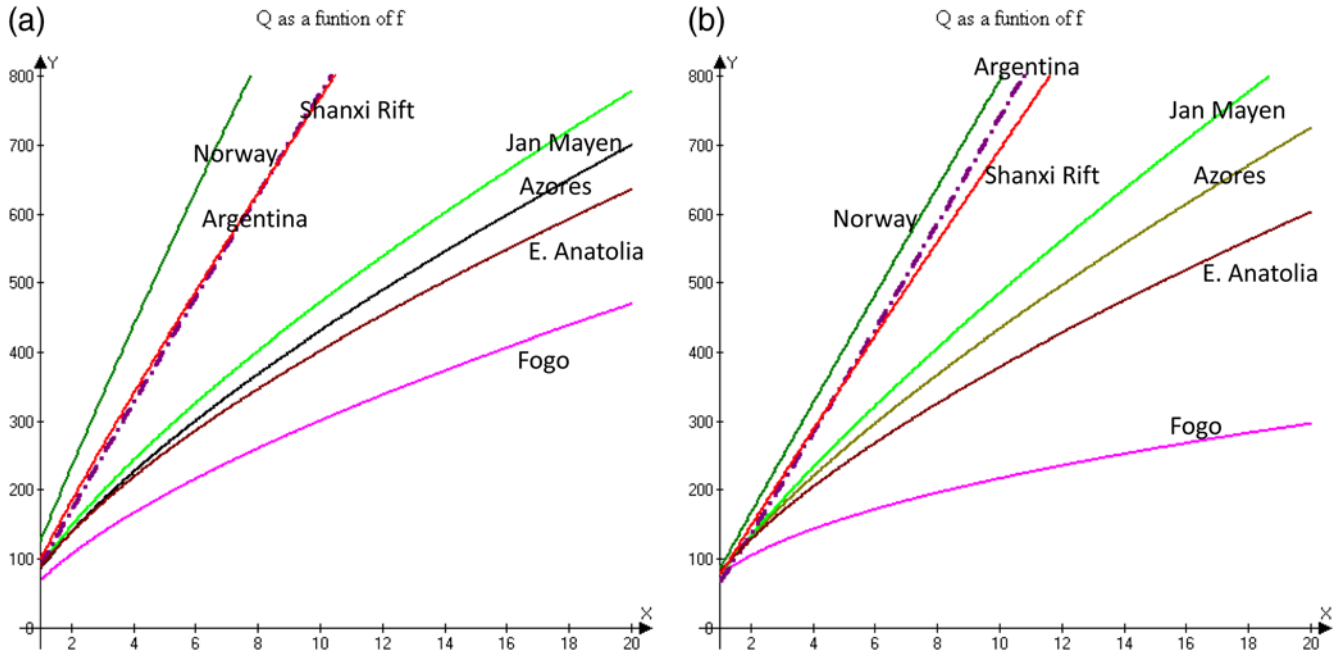

Figure 3. Coda Q as a function of frequency in the areas studied. (a) Results with our preferred parameters. (b) Results with more common alternative parameters. The color version of this figure is available only in the electronic edition.

time. All this indicates that our preferred parameters are optimal.

Global studies of *Lg* coda Q show pronounced regional variation at 1 Hz, higher Q_0 than our study and lower α, typically around 0.5. The higher Q_0 and lower α from *Lg* studies can be explained by the larger lapse time using *Lg* and fits the Gusev model. Mitchell *et al.* (2015) report Q_0 between 200 and 1000 for North America. Comparing these values with the values in Figure 5, it is seen that a Q_0 of 200–1000 would, in general, require lapse times of 100–1000 s. For eastern Canada, *Lg* Q_0 was around 1000 in the Mitchell *et al.* (2015) study while, for a lapse time of 20 s, Woodgold (1994) reported a coda Q_0 of 157. For the same area, Woodgold (1990) reports coda Q_0 of around 600, using a lapse time of around 150 s. This illustrates the difficulty in comparing Q_c with *Lg* coda Q.

The contrast in Q_0 between *Lg* coda Q and our coda Q is also due to measuring different things. At large lapse time, coda Q probably measures the intrinsic Q in the crust which can have large lateral variations. At short lapse times, it is thought that we measure both intrinsic and scattering Q with Q_{sc} being the dominant. At large distances, the *Lg* waves are dominated by total reflected *S* waves so only the crust is sampled while at short lapse times the angle of incidence is such that coda energy is lost to the mantle which significantly can affect Q_c (Margerin *et al.*, 1999). This might be a dominant effect at different sites and thus explain the smaller variation in Q_0 when observing coda Q at short distances versus *Lg* coda Q at large distances. The difference in high-frequency Q_c we observe between sites might be due to differences in both scattering (small scale scatters) and intrinsic Q.

In general, coda Q seems to vary little on a scale of a few hundred kilometers within a region of similar tectonics like between the different islands of the Azores or the north and central part of Argentina. However, in the Azores, the Fogo area stands out with low coda Q, particularly at high frequency. Using smaller lapse times and window lengths (and therefore smaller sampling areas) might better resolve regional differences, but this requires a dense network of stations and events. A smaller window also gives less stable results, particularly at low frequencies. Between regions of very different tectonics like the young (~1 million years) Azores and Jan Mayen regions and the older regions in Norway, the Shanxi rift system and Argentina, there is a significant difference in coda Q with the younger volcanic areas having the lowest coda Q. The Jan Mayen and the Azores areas are very similar in age and tectonics and have nearly identical coda Q. The similarity of the results for these two regions indicates that the coda Q method is reliable for comparing regions. It is interesting to note that eastern Anatolia shows somewhat lower coda Q than Jan Mayen and the Azores. This we interpret as due to the extremely fractured tectonics, relatively young age, and active volcanism.

The Fogo area shows an abnormally low coda Q, pointing to a relatively large body of volcanic material and/or a lot of fracturing. This area is also the seismically most active area in the Azores Islands (Silva *et al.*, 2012). Because we use a lapse time of 30 s and a window of 30 s, a quite large area is sampled (radius ~80 km), much larger than the Fogo volcanic area so the real coda Q in the Fogo area might be much lower.

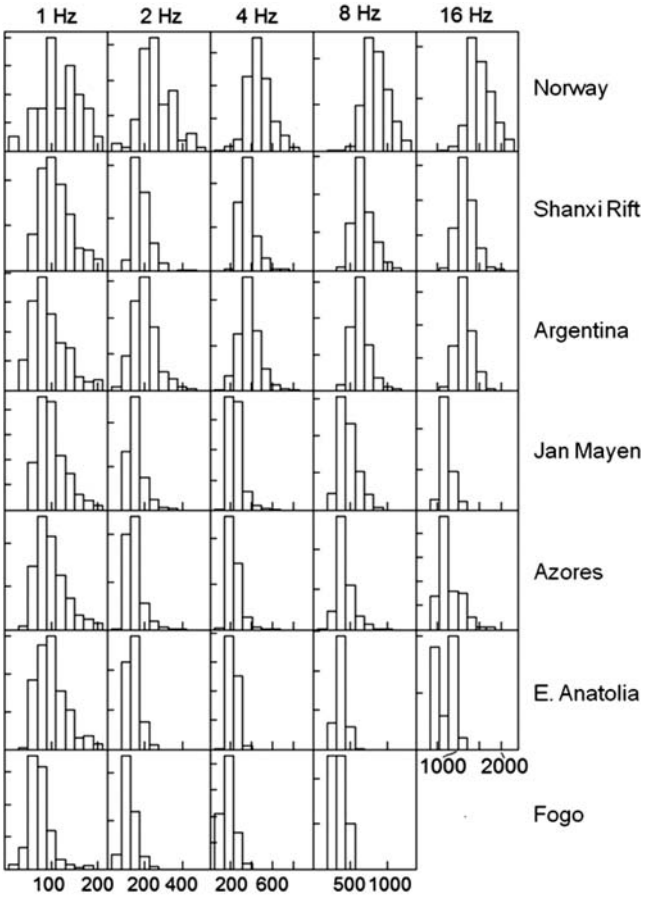

Figure 4. Distribution of coda Q values for each region and frequency band. The x axis is coda Q and the y axis the number of coda Q determinations in the shown coda Q intervals. The y axis is autoscaled.

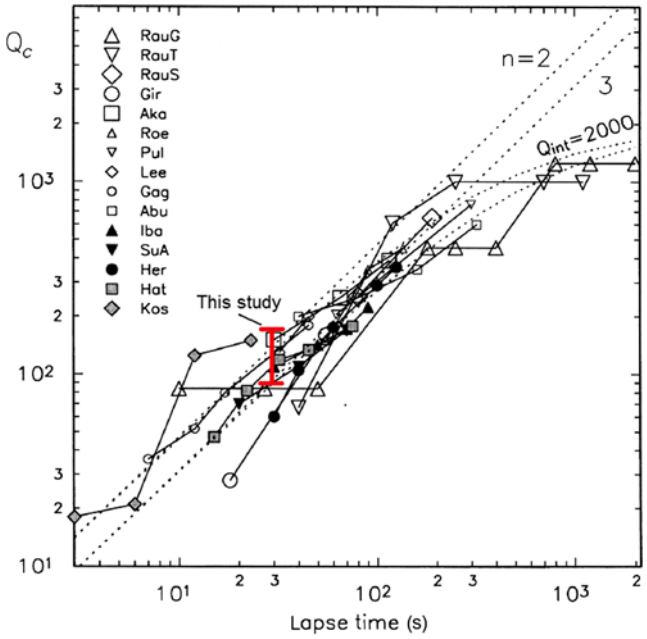

Figure 5. Comparing coda Q (Q_c) results from different tectonic provinces, as a function of lapse time. All coda Q values are at 1.5 Hz. The range of results from our study is indicated by a vertical line. Figure modified from Gusev (1995). Reference codes of individual studies are found in Gusev (1995). The color version of this figure is available only in the electronic edition.

Conclusions

Using identical processing parameters, the coda Q method can clearly distinguish very different tectonic environments while it is relatively insensitive to local variations unless they are very large like the case of the Fogo area. Tectonically similar areas also have very similar coda Q. The choice of parameters used in coda Q determination significantly affects the results, particularly at low frequencies. The regions can still be distinguished with less favorable parameters, but the absolute results are different. There is no answer to what is a correct coda Q since many different values can be obtained depending on the used processing parameters. We feel, however, that our choice of parameters fits the data better than those most commonly used. Despite the limitations in the CWD method, it is still widely used, however it is clearly necessary to use the same processing parameters and procedures when comparing coda Q for different areas. Using different parameters leads to quite different Q values, but the differences between the regions remain. Therefore, when using identical parameters, the CWD method will still be able to provide useful insight into differences in coda Q in different regions.

Data and Resources

The analysis presented here was performed using the SEISAN software (Havskov and Ottemöller, 1999) available at http://www.seisan.info (last accessed December 2015). The data used in this study are available at ftp.geo.uib.no/pub/seismo/REPORTS/CODAQ (last accessed December 2015). The site includes the software, all data used, results and parameter files used, and instructions for running the software to reproduce the results.

Acknowledgments

Data for this work were kindly provided by Instituto Português do Mar e da Atmosfera (IPMA), University of the Azores, the Norwegian National Seismic Network, Shanxi Seismic Network Center, National Institute for Seismic Prevention (INPRES), and Atatürk University. Figure 1 was plotted using the Generic Mapping Tools (GMT; Wessel *et al.*, 2013). Lars Ottemöller read the article and provided useful suggestions. We also want to thank the anonymous reviewers of the original version of this article for encouraging us to make a much more detailed study than originally submitted. The final reviewers also had many constructive suggestions.

References

Aki, K. (1980). Attenuation of shear-waves in the lithosphere for frequencies from 0.05 to 25 Hz, *Phys. Earth Planet. Int.* **21,** 50–60.

Aki, K., and B. Chouet (1975). Origin of coda waves: Source, attenuation and scattering effects, *J. Geophys. Res.* **80,** 3322–3342.

Akinci, A., J. M. Ibáñez, E. Del Pezzo, and J. Morales (1995). Geometrical spreading and attenuation of *Lg* waves: A comparison between Western Anatolia (Turkey) and southern Spain, *Tectonophysics* **250,** 47–50.

Akinci, A., L. Malagnini, R. B. Herrmann, and D. Kalafat (2014). High-frequency attenuation in the Lake Van region, eastern Turkey, *Bull. Seismol. Soc. Am.* **104,** 1400–1409.

Aydar, E., A. Gourgaud, I. Ulusoy, F. Digonnet, P. Labazuy, E. Sen, H. Bayhan, T. Kurttas, and A. U. Tolluoglu (2003). Morphological analysis of active Mount Nemrut stratovolcano, eastern Turkey: Evidences and possible impact areas of future eruption, *J. Volcanol. Geoth. Res.* **123,** 301–312.

Badi, G., E. Del Pezzo, J. M. Ibanez, F. Bianco, N. Sabbione, and M. Araujo (2009). Depth dependent seismic scattering attenuation in the Nuevo Cuyo Region (Southern Central Andes). *Geophys. Res. Lett.* **36,** L24307, doi: 10.1029/2009GL041081.

Bianco, F., M. Castellano, E. Del Pezzo, and J. M. Ibáñez (1999). Attenuation of short-period seismic waves at Mt. Vesuvius, Italy, *Geophys. J. Int.* **138,** 67–76.

Bianco, F., E. Del Pezzo, M. Castellano, J. Ibáñez, and F. Di Luccio (2002). Separation of intrinsic and scattering seismic attenuation in the Southern Apennine zone, Italy, *Geophys. J. Int.* **150,** 10–22.

Boztuğ, D., and Y. Harlavan (2008). K–Ar ages of granitoids unravel the stages of Neo-Tethyan convergence in the eastern Pontides and central Anatolia, Turkey, *Int. J. Earth Sci.* **97,** 585–599.

Calvet, M., and L. Margerin (2013). Lapse-time dependence of coda Q: Anisotropic multiple-scattering models and application to the Pyrenees, *Bull. Seismol. Soc. Am.* **103,** 1993–2010.

Calvert, A. T., R. B. Moore, J. P. McGeehin, and A. M. Rodrigues da Silva (2006). Volcanic history and $^{40}Ar/^{39}Ar$ and 14C geochronology of Terceira Island, Azores, Portugal, *J. Volcanol. Geoth. Res.* **156,** 103–115.

Carcole, E., and H. Sato (2010). Spatial distribution of scattering loss and intrinsic absorption of short-period S waves in the lithosphere of Japan on the basis of the Multiple Lapse Time Window Analysis of Hi-net data, *Geophys. J. Int.* **180,** 268–290.

Carvalho, A., C. Reis, and D. Vales (2015). Source and high-frequency decay parameters for the Azores region for stochastic finite-fault ground motion simulations, *Bull. Earthq. Eng.*, doi: 10.1007/s10518-015-9842-y.

Chen, Y. L., D. P. Li, Z. Wang, J. B. Liu, and C. Z. Liu (2012). History of formation and evolution on the crust around the Ordos Basin: Evidences from U-Pb dating and Hf isotopic composition of zircons, *Earth Sci. Front.* **19,** 147–166.

Del Pezzo, E., G. De Natale, G. Scarcella, and A. Zollo (1985). Q_c of three component seismograms of volcanic microearthquakes at Campi Flegrei volcanic area—southern Italy, *Pure Appl. Geophys.* **123,** 683–689.

Dobrynina, A. A. (2011). Coda-wave attenuation in the Baikal rift system lithosphere (2011), *Phys. Earth Planet. In.* **188,** 121–126.

Farrokhi, M., H. Hamzehloo, H. Rahimi, and M. Allamehzadeh (2015). Estimation of coda-wave attenuation in the central and eastern Alborz, Iran, *Bull. Seismol. Soc. Am.* **105,** 1756–1757.

Fehler, M., M. Hoshiba, H. Sate, and K. Obara (1992). Separation of scattering and intrinsic attenuation for the Kanto-Tokai region, Japan using measurements of S-wave energy vs. hypocentral distance, *Geophys. J. Int.* **108,** 787–800.

Fitch, F. J., D. L. Grasty, and J. A. Miller (1965). Potassium-Aagon ages and rocks from Jan Mayen and an outline of its volcanic history, *Nature* **208,** 1349–1351.

Ford, S. R., D. S. Dreger, K. Mayeda, W. R. Walter, L. Malagnini, and W. S. Phillips (2008). Regional attenuation in northern California: A comparison of five 1D Q methods, *Bull. Seismol. Soc. Am.* **98,** 2033–2046.

Frankel, A., and L. Wennerberg (1987). Energy-flux model of seismic coda: Separation of scattering and intrinsic attenuation, *Bull Seismol. Soc. Am.* **77,** 1223–1251.

Galluzzo, D., M. La Rocca, L. Margerin, E. Del Pezzo, and R. Scarpa (2015). Attenuation and velocity structure from diffuse coda waves: Constraints from underground array data, *Phys. Earth Planet. In.* **240,** 34–42.

Gusev, A. A. (1995). Vertical profile of turbidity and coda Q, *Geophys. J. Int.* **123,** 665–672.

Havskov, J., and K. Atakan (1991). Seismicity and volcanism of Jan Mayen Island, *Terra Nova* **3,** 517–526.

Havskov, J., and L. Ottemöller (1999). SEISAN earthquake analysis software, *Seismol. Res. Lett.* **70,** 532–534.

Havskov, J., and L. Ottemöller (2010). *Routine Data Processing in Earthquake Seismology*, Springer, The Netherlands, 347 pp.

Havskov, J., L. Kvamme, and H. Bungum (1986). Attenuation of seismic waves in the Jan Mayen Island area, *Geophys. Res.* **8,** 39–47.

Hellweg, M., P. Spudich, J. B. Fletcher, and L. M. Baker (1995). Stability of coda Q in the region of Parkfield, California: View from the U.S. Geological Survey Parkfield Dense Seismograph Array, *J. Geophys. Res.* **100,** 2089–2102.

Ibáñez, J. M., E. Del Pezzo, G. Alguacil, F. De Miguel, J. Morales, S. De Martino, C. Sabbarese, and A. M. Posadas (1993). Geometrical spreading function for short period S and coda waves recorded in southern Spain, *Phys. Earth Planet. In.* **80,** 25–36.

Ibáñez, J., E. Del Pezzo, F. De Miguel, M. Herraiz, G. Alguacil, and J. Morales (1990). Depth-dependent seismic attenuation in the Granada zone (southern Spain), *Bull. Seismol. Soc. Am.* **80,** 1232–1244.

Ibáñez, J. M., J. Morales, F. De Miguel, F. Vidal, G. Alguacil, and A. Posadas (1991). Effect of a sedimentary basin on estimations of Q_c and Q_{Lg}, *Phys. Earth Planet. In.* **66,** 244–252.

Jin, Y. K., X. J. Liang, H. Y. Jia, Y. W. Huo, J. P. Ma, and Q. X. Zhang (2012). Study on Q value of coda wave in the north of Shanxi based on Sato model, *Earthq. Res. Shanxi* **152,** 12–15 (in Chinese with English abstract).

Jin, Y. K., H. M. Zhao, and X. J. Liang (2008). Study on Q-value of coda wave of the earthquake swarm in Daixian of Shanxi, *Earthq. Res. Shanxi* **133,** 6–9 (in Chinese with English abstract).

Johnson, C. L., J. R. Wijbrans, C. G. Constable, J. Gee, H. Staudigel, L. Tauxe, V. H. Forjaz, and M. Salgueiro (1998). $^{40}Ar/^{39}Ar$ ages and paleomagnetism of São Miguel lavas, Azores, *Earth Planet. Sci. Lett.* **160,** 637–649.

Khan, P. K., K. Bhukta, and G. Tarafder (2015). Coda Q in eastern Indian shield, *Acta Geod. Geophys.* 1–14, doi: 10.1007/s40328-015-0129-1.

Kvamme, L. B., and J. Havskov (1989). Q in southern Norway, *Bull. Seismol. Soc. Am.* **79,** 1575–1588.

Li, B., J. Havskov, L. Ottemöller, and B. M. Sørensen (2015). New magnitude scales, M_L and spectrum based M_w for the area around Shanxi rift system, north China, *J. Seismol.* **19,** 141–158.

Mak, S., L. S. Chan, A. M. Chandler, and R. C. H. Koo (2004). Coda Q estimates in the Hong Kong region, *J. Asian Earth Sci.* **24,** 127–136.

Margerin, L., M. Campillo, N. M. Shapiro, and B. van Tiggelen (1999). Residence time of diffuse waves in the crust as a physical interpretation of coda Q: Application to seismograms recorded in Mexico, *Geophys. J. Int.* **138,** 343–352.

Matias, L., N. Dias, I. Morais, D. Vales, F. Carrilho, J. Madeira, J. Gaspar, L. Senos, and A. Silveira (2007). The 9th of July 1998 Faial Island (Azores, North Atlantic) seismic sequence, *J. Seismol.* **11,** 275–298.

Mayeda, K., S. Koyanagi, M. Hoshiba, K. Aki, and Y. Zeng (1992). A comparative study of scattering, intrinsic, and coda Q^{-1} for Hawaii, Long Valley, and central California between 1.5 and 15.0 Hz, *J. Geophys. Res.* **97,** 6643–6659.

Mitchell, B., J. L. Cong, and A. L. Jemberie (2015). Continent-wide maps of Lg coda Q for North America and their relationship to crustal structure and evolution, *Bull. Seismol. Soc. Am.* **105,** 409–419.

Mukhopadhyay, S., and J. Sharma (2010). Attenuation characteristics of Garwhal–Kumaun Himalayas from analysis of coda of local earthquakes, *J. Seismol.* **14,** 693–713.

Mukhopadhyay, S., J. Sharma, R. Massey, and J. R. Kayal (2008). Lapse-time dependence of coda Q in the source region of the 1999 Chamoli earthquake, *Bull. Seismol. Soc. Am.* **98,** 2080–2086.

Negi, S. S., A. Paul, A. Joshi, and Kamal (2015). Body wave crustal attenuation characteristics in the Garhwal Himalaya, India, *Pure Appl. Geophys.* **172,** 1451–1469.

Ning, Y. L., Y. K. Jin, and J. Z. Xu (2012). Q value of coda wave in Shanxi region based on Aki model, *Earthq. Res. Shanxi* **152,** 5–7 (Chinese with English abstract).

Rachman, A. N., T. W. Chung, K. Yoshimoto, and B. Son (2015). Separation of intrinsic and scattering attenuation using single event source in South Korea, *Bull. Seismol. Soc. Am.* **105,** 858–872.

Rahimi, H., K. Motaghi, S. Mukhopadhyay, and H. Hamzehloo (2010). Variation of coda wave attenuation in the Alborz region and central Iran, *Geophys. J. Int.* **181,** 1643–1654.

Rautian, T. G., and V. I. Khalturin (1978). The use of the coda for determination of the earthquake source spectrum, *Bull. Seismol. Soc. Am.* **68,** 923–948.

Reilinger, R. E., S. C. McClusky, M. B. Oral, R. W. King, M. N. Toksoz, A. Barka, I. Kinik, O. Lenk, and I. Sanli (1997). Global Positioning System measurements of present-day crustal movements in the Arabia–Africa–Eurasia plate collision zone, *J. Geophys. Res.* **102,** 9983–9999.

Richardson, T., H. Gilbert, M. Anderson, and K. D. Ridgway (2012). Seismicity within the actively deforming eastern Sierras Pampeanas, Argentina, *Geophys. J. Int.* **188,** 408–420.

Sanchez, G., R. Recio, O. Marcuzzi, M. Moreno, M. Araujo, C. Navarro, J. C. Suárez, J. Havskov, and L. Otemöller (2013). Argentinean national network of seismic and strong motion stations, *Seismol. Res. Lett.* **84,** 729–736.

Sato, H., M. C. Fehler, and T. Maeda (2012). *Seismic Wave Propagation and Scattering in the Heterogeneous Earth*, Second Ed., Springer-Verlag, Berlin, Germany, 494 pp.

Sertcelik, F. (2012). Estimation of coda wave attenuation in the East Anatolia fault zone, Turkey, *Pure Appl. Geophys.* **169,** 1189–1204.

Shapiro, N. M., M. Campillo, L. Margerin, S. K. Singh, V. Kostoglodov, and J. Pacheco (2000). The energy partitioning and the diffusive character of the seismic coda, *Bull. Seismol. Soc. Am.* **90,** 655–665.

Silva, R., J. Havskov, and C. Bean (2012). Seismic swarms, fault plane solutions and stress for São Miguel central region (Azores), *J. Seismol.* **16,** 389–407.

Singh, C., S. Mukhopadhyay, S. Singh, P. Chakrabort, and J. R. Kayal (2015). Study of lapse time dependence coda Q in the Andaman Islands using the aftershocks of the 2002 earthquake (M_w 6.5), *Nat. Hazards* **75,** 779–793.

Steck, L. K., W. A. Prothero, and J. Scheimer (1989). Site-dependent coda Q at Mono Craters, California, *Bull. Seismol. Soc. Am.* **79,** 1559–1574.

Torske, T. (1977). The south Norway Precambrian region—A Proterozoic cordilleran-type orogenic segment, *Norsk Geologisk Tidsskrift* **57,** 97–120.

Vidales-Basurto, C. A., R. R. Castro, C. I. Huerta, D. F. Sumy, J. B. Gaherty, and J. A. Collins (2014). An attenuation study of body waves in the south-central region of the Gulf of California, México, *Bull. Seismol. Soc. Am.* **104,** 2027–2042.

Vujovich, G. I., C. R. van Staal, and W. Davis (2004). Age constraints on the tectonic evolution and provenance of the Pie de Palo complex, Cuyania Composite Terrane, and the Farnatinian Orogeny in the Sierra de Pie de Palo, San Juan, Argentina, *Gondwana Res.* **7,** 1041–1056.

Wessel, P., W. H. F. Smith, R. Scharroo, J. F. Luis, and F. Wobbe (2013). Generic Mapping Tools: improved version released, *Eos Trans. AGU* **94,** 409–410.

Woodgold, C. R. D. (1990). Estimation of coda Q in eastern Canada, *Bull. Seismol. Soc. Am.* **80,** 411–429.

Woodgold, C. R. D. (1994). Coda Q in the Charlevoix, Quebec, Region: Lapse-time dependence and spatial and temporal comparisons, *Bull. Seismol. Soc. Am.* **84,** 1123–1131.

Wu, L. (1982). Shanxi seismic network, *Earthq. Res. Shanxi* **1,** 2–19 (in Chinese with English abstract).

Xie, J., and O. W. Nuttli (1988). Interpretation of high-frequency coda at large distances: Stochastic modeling and method of inversion, *Geophys. J.* **95,** 579–595.

Xu, X. W., X. Y. Ma, and Q. D. Deng (1993). Neotectonic activity along the Shanxi rift system, China, *Tectonophysics* **219,** 305–325.

Yun, S., W. S. Lee, K. Lee, and M. H. Noh (2007). Spatial distribution of coda Q in South Korea, *Bull. Seismol. Soc. Am.* **97,** 1012–1018.

Zelt, B. C., N. T. Dotzev, R. M. Ellis, and G. C. Rogers (1999). Coda Q in southwestern British Columbia, Canada, *Bull. Seismol. Soc. Am.* **89,** 1083–1093.

Department of Earth Science
University of Bergen
Allegaten 41
5007 Bergen, Norway
(J.H., M.B.S., B.L.)

Instituto Português do Mar e da Atmosfera
Rua C do Aeroporto
1749-077 Lisboa
Portugal
(D.V.)

Atatürk University
Earthquake Research Center
Refik Saydam Caddesi
Kiremitlik Tabya Mevkisi
25240 Erzurum, Turkey
(M.Ö.)

Instituto Nacional de Prevencion Sismica
Roger Balet 47 (norte)
C.P. 5400, San Juan, Argentina
(G.S.)

Manuscript received 16 March 2016;
Published Online 24 May 2016